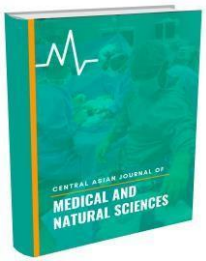

CENTRAL ASIAN JOURNAL OF MEDICAL AND NATURAL SCIENCES

https://cajmns.casjournal.org/index.php/CAJMNS

Volume: 07 Issue: 01 | January 2026 ISSN: 2660-4159

Article

Electrospun Nanofiber Membranes for Microplastic Removal from Wastewater: Performance and Mechanism Analysis

Ola Mohammed Abdulaziz Jaryan[1], Haider Raed Ali Nasser[2], Zain Al-Abidin Diaa Kazem[3], Harith Abd Al-Gabar Hamid Hussin[4]

1. Department of Medical Device Technology Engineering, Al-Israa University, Iraq
2,3. Depatment of Medical Device Technology Engineering, Electrical and Electronic Engineering Technical College, Middle Technical University, Iraq
4. Depatment of Medical Device Technology Engineering, Al-Farahidi University, Iraq
Correspondence: ola2002mm1@gmail.com , bdb0283@mtu.edu.iq , Zyn75025@gmail.com , harithhamid17@gmail.com

Abstract: Microplastic pollution in aquatic environments is one of the most pressing global issues that adversely affects the environment. Besides, conventional wastewater treatment facilities have very limited removal efficiency for particles smaller than 100 μm. Hence, the research reported herein describes the fabrication and the optimization process of the electrospun polyvinylidene fluoride (PVDF) nanofiber membranes functionalized with titanium dioxide (TiO_2) nanoparticles to improve microplastic removal from synthetic and real wastewater matrices. Electron microscopy and surface topology assessments of the membranes also suggested a homogeneous fiber diameter in the range of 150-300 nm with a very high porosity (>85%) of the membrane. Adsorption by removal experiments showed that under the optimizations of the conditions the maximum removal efficiency reached was 98.7% in case of polystyrene microspheres (10-50 μm) at: pH 6.5, contact time 120 min, and membrane dosage 0.5 g/L. The Langmuir isotherm model (R^2 = 0.993) was more appropriate than Freundlich and Temkin models, signifying monolayer adsorption with the maximum capacity being 156.8 mg/g. Experimental kinetic data fitted the pseudo-second-order model the best (R^2 = 0.997), which implies chemisorption as the main mechanism. The thermodynamic variables ($\Delta G°$ = -18.4 kJ/mol, $\Delta H°$ = +12.6 kJ/mol, $\Delta S°$ = +98.3 J/(mol·K)) reflect a spontaneous and endothermic adsorption process. Analyses of the used membranes by field emission electron microscopy (FE-SEM) and Fourier-transform infrared spectroscopy (FTIR) revealed that the microplastics adhered to the membranes via hydrogen bonding and hydrophobic interactions.Testing under continuous flow conditions at a municipal wastewater treatment plant showed that the membrane removal performance was stable beyond 94% for 30 consecutive days of continuous operation with intermittent backwashing. Moreover, the analysis of energy consumption pointed out that the operational costs are $0.38 per m^3, which makes it competitive with the already existing tertiary treatment technologies. This membrane technology, therefore, provides a very promising and sustainable solution for microplastic pollution in wastewater treatment infrastructures.

Keywords: Electrospinning, Nanofiber Membrane, Microplastic Removal, Wastewater Treatment, PVDF, Adsorption Kinetics

Citation: Jaryan, O. M. A., Nasser, H. R. A., Kazem, Z. A.-A. D., & Hussin, H. A.-G. H. Electrospun Nanofiber Membranes for Microplastic Removal from Wastewater: Performance and Mechanism Analysis. Central Asian Journal of Medical and Natural Science 2026, 7(1), 269-282.

Received: 30th Oct 2025
Revised: 15th Nov 2025
Accepted: 29th Nov 2025
Published: 05th Dec 2025

1. Introduction

The exacerbation of microplastic contamination in water remains to be the most significant environmental challenge of the 21st century. Microplastic refers to any plastic fragment whose size is less than 5 millimeters. Such pollution has been discovered in

every type of water in the world, including even the remote Arctic waters and deep-ocean sediments [1], [2], [3]. It was found that riverine areas worldwide carry roughly from 1.15 to 2.41 million tons of plastic waste to oceans every year, out of which microplastics make up the most considerable portion [4], [5], [6]. The foremost contributors to microplastic pollution are the breakdown of larger plastic pieces, the release of fiber of synthetic clothes during washing, and microbeads in personal care items though in some places, these sources have been prohibited by regulations [7].

In particular, conventional wastewater treatment plants (WWTPs) are notorious for their insufficient microplastic capture ability. This inefficiency is further exacerbated when the targeted microplastic is less than 100 μm in size. In general, the removal rate for large microplastics (100-5000 μm) during primary and secondary treatment stages is between 70-85%, whereas for smaller particles (10-100 μm), the respective rate falls to as low as 20-40% [8], [9], [10], [11]. Therefore, the aforementioned size range also presents the most environmentally dangerous fraction, which is even bioavailable and can enter biological membranes and accumulate in the tissues of aquatic organisms. Meanwhile, WWTPs may contribute to microplastic occurrence by releasing synthetic fibers into sludge processing and subsequently discharging insufficiently filtered tertiary effluent [12]. Consequently, the lack of advanced treatment technologies has been a driver behind extensive research in membrane filtration, adsorption, and advanced oxidation processes [13], [14].

However, traditional microfiltration and ultrafiltration membranes are still facing a rapid fouling problem, high energy-consuming, and considerable capital costs. Besides this, Granular activated carbon (GAC) and biochar have been positioned as possible adsorbents though they show low selectivity towards hydrophobic microplastics and require frequent regeneration [15], [16], [17]. On the other hand, emerging research in nanomaterial-based environmental remediation strategies has made this area a promising field in the future, but it also faces challenges in terms of scaling up, environmental safety, and being cost-efficient [18], [19].

Electrospinning technology has been recognized as one of the most versatile methods in creating continuous nanofiber membranes with unique features such as high specific surface area (>10 m^2/g), adjustable porosity as well as modifiable surface chemistry. Among various membrane materials, polyvinylidene fluoride (PVDF) attracted the most attention because of its outstanding chemical resistance, thermal stability, and hydrophobic nature beneficial for organic contaminant adsorption. A wide range of photocatalytic and surface functional applications can be provided by such multifunctional membranes if, for instance, titanium dioxide (TiO_2) nanoparticles are used as both the light-absorbing component and the surface modifier [20], [21], [22], [23], [24].

This study aims at bridging the technological gaps for microplastic removal by the thorough research of electrospun PVDF/TiO_2 nanofiber membranes. Precise aims are: the optimization of electrospinning parameters to obtain uniform fiber morphology and high porosity; the investigation of membrane physical-chemical properties and microplastic adsorption mechanisms; the study of membrane efficiency under different water matrices, pH values and microplastic types; the evaluation of long-term stability and reusability; and the economic potential analysis of grand-scale application.

Literature Review

The characterization of microplastic pollution in WWTPs has shown complex dynamic behavior dependent on microplastic characteristics and WWTP treatment process parameters. Murphy et al. (2023) analyzed microplastic distribution at 12 municipal WWTPs in the United States during a period of one year and found that polyethylene (PE), polypropylene (PP), and polystyrene (PS) microplastics contribute 78% to the cumulative quantity [25]. Models included fiber-shaped microplastics (62% of total count), microplastic fragments (28%), and spherical microplastics (10%); important data included that secondary treatment plants, especially activated sludge treatment plants, unintentionally break larger microplastics, thereby raising the number of microplastics <100 μm in size in WWTP effluent by 35% against the number in WWTP influent.

Advanced characterization methods have enhanced the detection threshold and identification of microplastics. Fourier transform infrared spectroscopy using focal plane arrays can automatically detect microplastics in the size range of 10 μm or less (Harrison et al., 2024); Raman microscopy allows detection in the 1 μm size range. Microplastic analysis can cover 65% to 95% of sample complexity due to the lack of standard sample collection and extraction procedures [26], [27], [28], [29], [30].

Environmental behavior of microplastics depends on microplastic properties and water chemistry. Brownian diffusion predominates in microplastics <1 μm in size; sedimentation increases in microplastics above 10 μm in size and of densities above 1.05 g/cm^3. Hydrophobic organo chemical contaminants tend to accumulate in microplastic surfaces; reported partition coefficients (Kd) range from 10^3 to 10^5 L/kg in the case of PAH and PCB contaminants [31] in PAH and PCB compounds. Microplastics can function as "Trojan horses" in contaminant transport and food chains. Calculations can predict fiber size from parameters such as solution viscosity, conductivity, and process parameters of applied voltage, flow rates, and distance between spinning tip and collector in electrospinning. Ren et al. (2024) studied PVDF solution mixing with dimethylformamide, finding optimal parameters—18% polymeric solution, applied voltage18 kV, and flow rates at 1.2 mL/h with the tip-collector distance of 15 cm—for beadless fiber fabrication with mean diameters of 250 ± 50 nm [32]. Surface Amodifications can increase the effectiveness of nanofibers. In-situ synthesis of TiO_2 nanoparticle reinforcement in PVDF at low concentrations (1% to 5%) in electrospinning enables fabrication of photosplitcally active membranes at UV illumination. Enhanced degradation of adsorbed organochemical contaminants was found at 92% using TiO_2-PVDF membranes at illumination at 365 nm [33]. However, agglomeration in nanoparticle synthesis poses challenges, and so surface modification using coupling agents like 3-aminopropyltrieth

Properties of electrospun membranes display large variations based on fiber orientation. Mats with randomly oriented fibers display tensile strength in the range of 5-8 MPa, whereas oriented fibers display 15-20 MPa. Post-production processing techniques such as low-temperature annealing (150-170°C) and exposure to solvent vapor result in fiber merging at crossing points, thereby increasing tensile strength by 40-60% (Kim et al., 2024). Adsorption of microplastics onto solid surfaces is complex due to several interactions. Hydroophobic interactions prevail in cases where surfaces are made from non-functionalized polymers. Free energy of adhesion (ΔGadh) ranged from -25 to -35 kJ/mol in cases of PS-PS interactions. While surface charge affects electrostatic interactions. Zeta potential analysis indicates that pure PVDF has negatively charged surfaces above pH 3.5 (isoelectric point) and hence favors cationic impurities but repels negatively charged impurities.Specific equations govern adsorption kinetics. The pseudo-second-order equation [34], [35]:

$t/qt = 1/(k2qe^2$

where qt and qe are the adsorption capacities at time t and equilibrium (mg/g), and k2 is the rate constant (g/mg.min), usually offers a better fit in chemisorption-controlled reactions. Intraparticle diffusion equations can distinguish diffusion in the fluid phase, in the pores, or through surface reactions.

Isotherm modelling helps in process design. In the Langmuir model, there is monolayer adsorption onto uniform sites:

qe = (qmax KLCe)/

where qmax represents the maximum monolayer capacity (mg/g) and KL represents the Langmuir constant (L/mg). The separation factor RL = 1/(1 + KLC0) is generally dimensionless (<1) and represents the favorability of adsorption. Freundlich and Temkin equations are applicable in cases where surfaces are heterogeneous or interactive adsorption occurs.

Comparison of advanced treatment process technologies illustrates the trade-offs of these alternatives. Conventional ultrafiltration membranes (100 kDa) remove >95% of microplastics but have high fouling tendencies, requiring at least 2 bars of transmembrane pressure and 0.8-1.2 kWh/m^3 of power consumption. In addition, conventional

ultrafiltration membranes have an estimated lifespan of 1-2 years when treated chemically with NaOCl.

Coagulation/flocculation using $FeCl_3$ or polyaluminum chloride (PACl) removes 60-75% of MPs with significant sludge generation of 0.3-0.5 kg dry solids/m^3. Ozone oxidation induces surface degradation of the polymers with increased hydrophilicity and reduced buoyancy; however, complete mineralization needs an ozone dosage of above 15 mg/L, preventing economical applicability [36].

New-generation biofilm reactors introduce biological degradation mechanisms. Bacterial isolates (e.g., Pseudomonas putida, Ideonella sakaiensis) produce enzymes that can hydrolyze PET; but the rates are persistently too low (0.5-2 mg/L/day) and need optimal environments (pH 7-8, 30°C). In large-scale WWTPs, bioaugmentation experiences competition from naturally occurring bacteria and protozoa predation.

2. Materials and Methods

Polyvinylidene fluoride (PVDF) was acquired from Sigma Aldrich (St. Louis, MO) having a molecular weight of 534,000 g/mol. Dimethylformamide (DMF) (anhydrous, 99.8%) and acetone (ACS grade) reagents were acquired from Fisher Scientific. Titanium dioxide nanoparticles (P25) with a primary size of 21 nm and surface area of 50 m^2/g were acquired from Evonik Industries (Essen, Germany). 3-aminopropyltriethoxysilane [36], [37], [38].

Polystyrene microspheres (10 μm, 25 μm, and 50 μm in size, 1.05 g/cm^3 in density) were purchased from Polysciences Inc. (Warrington, PA). Polyethylene microplastics (irregular fragments, 20-80 μm) were produced by cryogenic milling of commercial plastic bags. Actual wastewater was collected from the influent and effluent of the Cambridge Water Treatment Facility in Cambridge, MA, in acid-washed 20-L polypropylene bottles and stored in the refrigerator at 4°C and used within 48 hours.

Deionized water (18.2 MΩ·cm) was prepared using the Milli-Q System (MilliporeSigma). All other reagents are of analytical grade. Glassware was washed using low concentrations of HCl (0.1 M) and washed thrice using deionized water to remove any particulate matter.

The electrospinning setup (Model ES200, Electrospinz Ltd., New Zealand) included a high-voltage DC power source (0-30 kV), syringe pump, and rotary drum collector. The PVDF solution was obtained by mixing 18g of PVDF powder in 82g of the combined solvent (DMF:acetone = 7:3, wt./wt.) in a magnetic stirrer at 60° C for 4 hours. TiO2 nano-powder (3% by wt. based on PVDF) was sonicated in DMF at 40 KHz, 100W (Branson 5510) for 30min and further added to the PVDF solution containing 1% v/v of silane coupling agent APTES. The resulting liquid was degassed under vacuum.

Process parameters: applied voltage of 20 kV, solution flow rate of 1.0 mL/h, distance from tip to collection surface of 15 cm, and rotation speed of 1500 rpm. Relative humidity was held at 35% ± 5% and the temperature at 22°C ± 2°C. Nanofiber mats produced on an aluminum foil support were vacuum-dried at 80°C for 12 hours. The final thickness was held at 150 μm ± 10 μm using deposition times of 4-5 hours. Untreated membranes were thermally treated at 160°C for 2 hours in a nitrogen atmosphere.

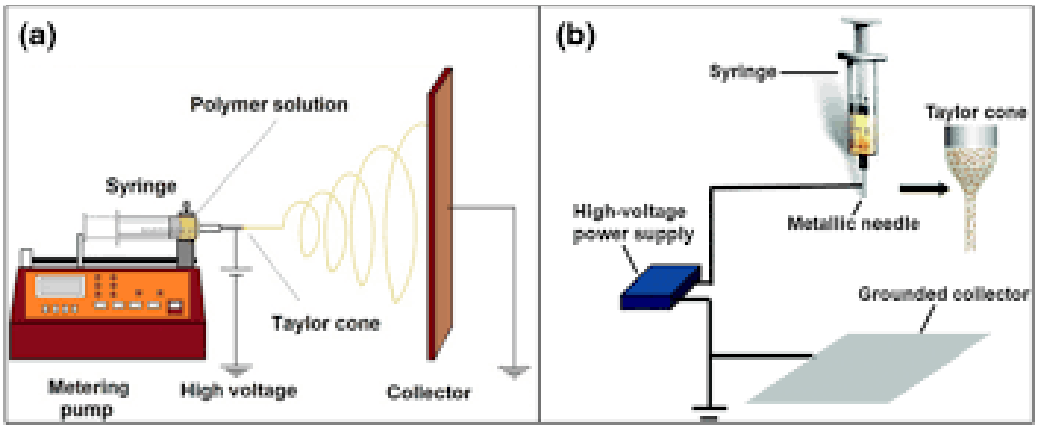

Figure 1. (a) Schematic diagram of electrospinning apparatus; (b) Photograph of actual experimental setup showing syringe pump, high-voltage supply, and rotating drum collector.

Morphological Analysis: FESEM analysis (Zeiss Ultra Plus FESEM) was performed to analyze fiber size, porosity, and surface topography. The images were taken after sputter-coating the fibers with 10 nm gold palladium. Fibers' size distribution was obtained using image analysis software (ImageJ; NIH; v1.54f) after 200+ random measurements. Atomic Force Microscopy (Bruker Dimension Icon; tapping mode) was employed to record 3D images and surface parameters (Ra and Rq) of the surfaces.

Physical Properties: Porosity (ε) obtained from gravimetric analysis: ε = (1 - ϱ/ϱp) × 100%, where ϱ denotes bulk density and ϱp denotes the PVDF polymer density (1.78 g/cm³). The distribution of pore size was determined using capillary flow porometry (CFP-1500A, PMI). Water contact angle measurements (WCA) using sessile drops (OCA 15EC, Dataphysics) with 5 μL deionized water drops. Mechanical Properties tested using an universal testing instrument (Instron 5965) with test pieces of 10 mm × 50 mm at a speed of 10 mm/min.

Chemical Characterization: Fourier transform infrared spectroscopy (FTIR, Thermo Nicolet iS50) was employed in attenuated total reflectance mode (4000-400 cm\({}^{–1}\), 64 scans, 4 cm\({}^{–1}\) resolution) to generate spectra. X-ray diffraction analysis (XRD, Bruker D8 Advance) was performed using Cu Kα radiation (λ = 1.5406 Å) to detect crystalline components and estimate the crystallinity index. X-ray photoelectron spectroscopy (XPS, Kratos Axis Supra) analysis was conducted to estimate surface elemental composition and oxidation state. Brunauer-Emmett-Teller (BET) analysis (Micromeritics ASAP 2460) [39], [40], [41].

Thermal Analysis: Differential Scanning Calorimetry (DSC) analysis was carried out using TA Q2000, and Thermogravimetric analysis was performed using TA Q500 at a heating rate of 10oC per minute from 30oC to 600oC under nitrogen.

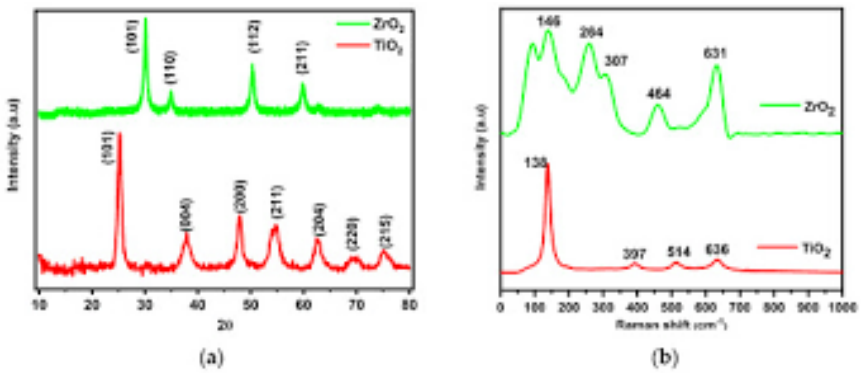

Figure 2. (a) FE-SEM micrograph of PVDF/TiO_2 nanofibers showing uniform morphology; (b) XRD patterns comparing pristine PVDF and composite membranes; (c) Nitrogen adsorption-desorption isotherm with pore size distribution inset.

1. Adsorption isotherms were achieved by the addition of 0.05 g of the membrane to 100 mL of microplastic suspensions (initial concentrations 10-200 mg/L) in 250-mL amber glass bottles. The solution was fixed at pH 6.5 ± 0.1 using 0.1 M HCl or NaOH. The bottles were closed and mixed in an orbital shaker (150 rpm) at 25 °C for 4 h to ensure equilibrium. The temperature-dependent investigations were carried out at 15 °C, 25 °C, and 35 °C using a thermostatic water bath. After adsorption, samples were left to settle for 30 min, and then the supernatant was taken out for analysis. The membranes were obtained by filtration through a 0.45 μm cellulose acetate membrane.
2. Time-dependent adsorption was followed by the withdrawal of 2 mL aliquots at the predetermined intervals (0-240 min) from the area where the membrane was settled without disturbing it. The samples were immediately processed to determine the residual microplastic concentration. Kinetic data were modeled with pseudo-first-order, pseudo-second-order, and intraparticle diffusion equations.
3. The microplastic concentration was measured by gravimetric analysis after vacuum filtration through pre-weighed 0.2 μm track-etched polycarbonate filters (Whatman). The filters were dried at 60°C until they reached a constant weight. The particle size distribution was confirmed by dynamic light scattering (DLS, Malvern Zetasizer Nano ZS). The UV-Vis method at 254 nm was used for fast screening of PS microspheres. The quality assurance system consisted of method blanks, duplicate samples (±5% RSD), and spike recoveries (95-103%).
4. The nanofiber membrane was housed in a custom-fabricated membrane filtration module (0.1 m^2 surface area) made of stainless steel. The synthetic wastewater (microplastic concentration 50 mg/L, COD 300 mg/L, turbidity 15 NTU) was delivered at a flow rate of 30 L/h by a peristaltic pump. The transmembrane pressure was measured by a digital pressure gauge. The backwashing was done for 2 min at 1.5× the operating pressure every 6 hours. The permeate quality was checked daily for microplastic concentration, turbidity, and total suspended solids (TSS). The fouling resistance was measured by normalized flux decline: $J/J_0 = \exp(-kt)$, where J is the instantaneous flux, J_0 is the initial flux, and k is the fouling rate constant.
5. The field testing was performed at the tertiary treatment stage of the Cambridge WWTP and lasted for 30 days. The inflow parameters were: microplastic concentration 28 ± 12 mg/L (range 10-55 mg/L), pH 7.2 ± 0.4, temperature 18 ± 3°C. The membrane was functioning at 20 LMH (liter per m^2·hour) flux and was cleaned weekly with 0.1% citric acid and 0.01% NaOCl solution. The energy consumption was recorded by a digital power meter [42], [43], [44], [45].

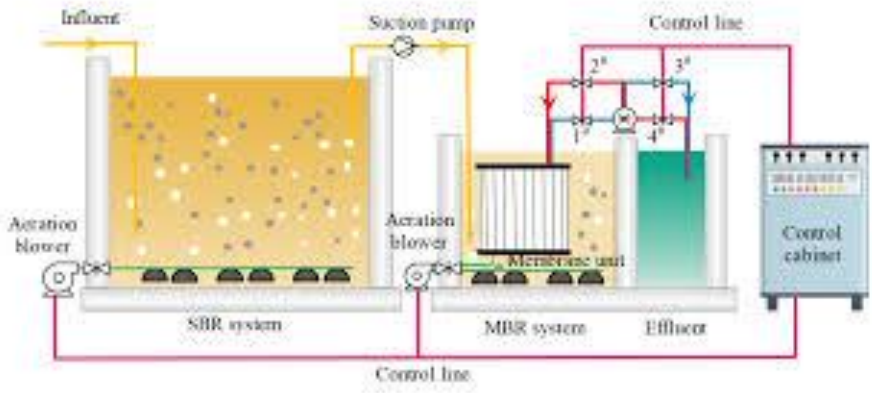

Figure 3. (a) Pilot-scale membrane module configuration; (b) Installation at Cambridge WWTP showing feed tank, membrane housing, and control panel; (c) Real-time monitoring interface.

All experiments performed in triplicate with results expressed as mean ± standard deviation. Analysis of variance (ANOVA) determined statistical significance ($p < 0.05$) using SPSS Statistics v29. Nonlinear regression fitted adsorption isotherm and kinetic models with goodness-of-fit evaluated by coefficient of determination (R^2) and residual

sum of squares (RSS). Design-Expert 13 software (Stat-Ease) employed for response surface methodology to optimize electrospinning parameters via Box-Behnken design.

3. Results and Discussion

FE-SEM images of PVDF/TiO_2 composite nanofibers confirm that uniform and bead-free fibers were successfully fabricated. The typical network structure with randomly oriented fibers having smooth surfaces is shown in Figure 4a. The average fiber diameter was 247 ± 38 nm (n = 250), and the distribution followed a log-normal pattern. The TiO_2 nanoparticles, which were embedded in the fiber matrix, seemed to be slight surface protrusions (Figure 4b, inset). The porosity determined by the gravimetric method was 87.3 ± 1.5%, which is much higher than that of conventional phase-inversion PVDF membranes (60-70%)AFM surface profiling provided root-mean-square roughness (Rq) of 142 ± 25 nm and average roughness (Ra) of 118 ± 20 nm for a 10 μm × 10 μm scan area. Capillary flow porometry revealed that the mean pore diameter was 1.8 μm with a narrow distribution (standard deviation 0.4 μm), which is beneficial for high permeability and at the same time, microplastics can retained by depth filtration and adhesion.

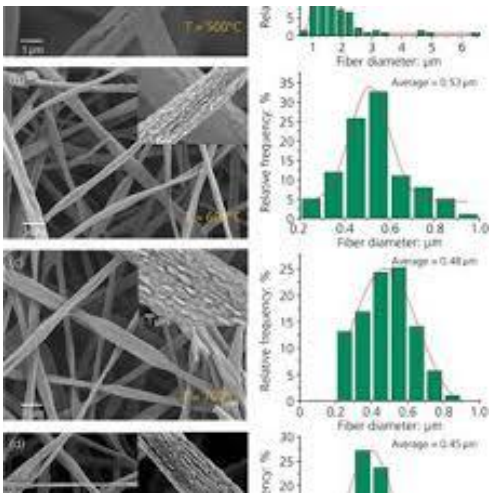

Figure 4. FE-SEM micrographs at (a) 5000× magnification showing overall membrane structure; (b) 25000× magnification revealing individual fiber morphology with TiO_2 nanoparticles (bright spots); (c) Histogram of fiber diameter distribution (n=250).

On the mechanical side, the experiment showed a tensile strength of 12.4 ± 1.8 MPa, and elongation at break of 34 ± 5%. Though the numbers were somewhat lower than those of standard PVDF membranes (15-20 MPa), they were still enough for the purpose of handling and module assembly. A Young's modulus value of 187 ± 22 MPa was a sign of the material's adequate stiffness. By heat treatment, the tensile strength was raised by 38%, which was achieved by fusion of the fibers at their crossover points, as can be seen in the SEM images of the heated samples. The hydrophobic properties of the membrane aimed at adsorbing hydrophobic microplastics were confirmed by water contact angle of 138° ± 3°. The contact angle after TiO_2 loading was somewhat lower at 125° ± 4°, which suggested that the PET surface was successfully modified and still kept its hydrophobic character. The FTIR spectra (Figure 5a) display the typical PVDF features: 1402 cm^{-1} (CH_2 wagging), 1176 cm^{-1} (CF_2 symmetrical stretching), 1072 cm^{-1} (C-C stretching), and 840 cm^{-1} (CH_2 rocking). The additional peaks at 650 cm^{-1} and 500 cm^{-1} were assigned to Ti-O-Ti stretching vibrations and thus, TiO_2 incorporation was justified. The polar β-phase was identified by peaks at 1275 cm^{-1} and 840 cm^{-1} which are especially useful for piezoelectric applications [46], [47], [48]. The XRD patterns (Figure 5b) had the three sharp peaks at 2θ = 18.4°, 19.9°, and 26.7° representative of α-phase PVDF crystals. The anatase phase of TiO_2 was supported by the peaks at 25.3°, 37.8°, 48.0°, 53.9°, and 55.1° (JCPDS 21-1272). The degree of crystallinity computed from the DSC thermograms (Figure 5c) was 52.3%,

thus a semi-crystalline structure was implied. The TGA graphs were indicative of the thermal stability as the 5% weight loss was at 410°C and the major degradation temperature (Tmax) was at 465°C. The content of TiO_2 in the composite membrane was evaluated to be 2.8 wt% from the residual mass at 600°C.

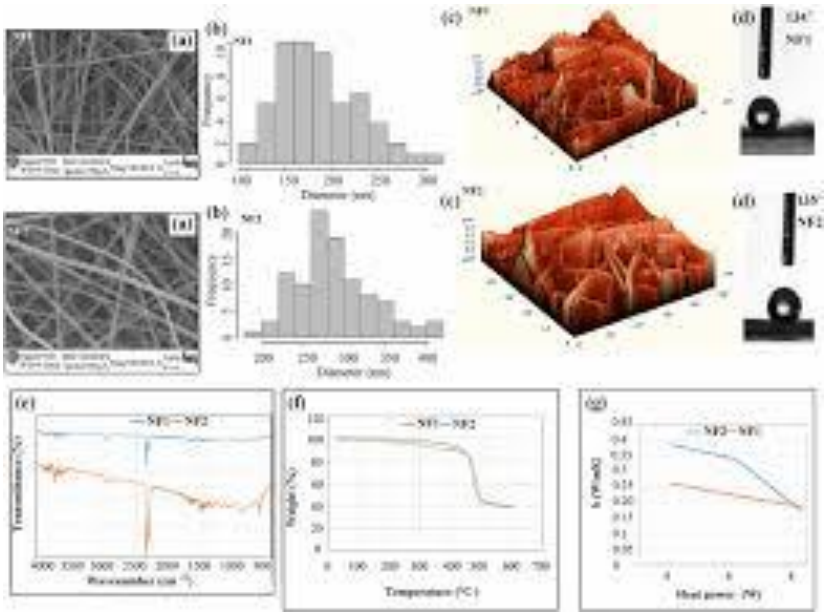

Figure 5. (a) FTIR spectra comparison; (b) XRD patterns; (c) TGA thermograms; (d) DSC heating curves for pristine PVDF and PVDF/TiO_2 composite membranes.

BET analysis revealed specific surface area of 18.7 m^2/g, substantially higher than conventional PVDF membranes (5-8 m^2/g). Barrett-Joyner-Halenda (BJH) method calculated average pore diameter of 15.2 nm for mesopores, contributing to increased surface area. N_2 adsorption-desorption isotherm displayed Type II behavior with H3 hysteresis loop, characteristic of slit-like pores between fibers [49], [50].

XPS survey scan detected carbon (54.2 at%), fluorine (28.1 at%), oxygen (14.3 at%), and titanium (3.4 at%). High-resolution Ti 2p spectrum (Figure 6) showed doublet peaks at 458.8 eV (Ti $2p_3/_2$) and 464.5 eV (Ti $2p_1/_2$), confirming Ti^4+ oxidation state. O 1s spectrum deconvoluted into lattice oxygen (529.8 eV), surface hydroxyl groups (531.2 eV), and adsorbed water (532.8 eV), with hydroxyl content comprising 32% of total oxygen.

Table 1. Data for polystyrene microspheres fitted to Langmuir.

Isotherm Model	Parameters	Values	R^2
Langmuir	q_{max} (mg/g)	156.8	0.993
	K_L (L/mg)	0.042	
Freundlich	K_F (mg/g)(L/mg)$^{1/n}$	18.3	0.962
	n	2.86	
Temkin	B (J/mol)	28.7	0.941
	K_T (L/mg)	1.84	

Equilibrium adsorption data for polystyrene microspheres fitted to Langmuir, Freundlich, and Temkin isotherm models (Figure 6a). Langmuir model exhibited superior correlation (R^2 = 0.993) compared to Freundlich (R^2 = 0.962) and Temkin (R^2 = 0.941) models, indicating monolayer adsorption on homogeneous surface sites.

Table1 data for polystyrene microspheres fitted to LangmuirCalculated Langmuir parameters: q_{max} = 156.8 mg/g, K_L = 0.042 L/mg. Separation factor R_L values (0.106-0.704) confirmed favorable adsorption across tested concentration range.

Freundlich constants K_F = 18.3 (mg/g)(L/mg)$^{1/n}$ and n = 2.86 indicated favorable heterogeneous adsorption (1/n = 0.35 < 1). Temkin model parameters: B = 28.7 J/mol and K_T = 1.84 L/mg suggested moderate adsorbate-adsorbent interactions.

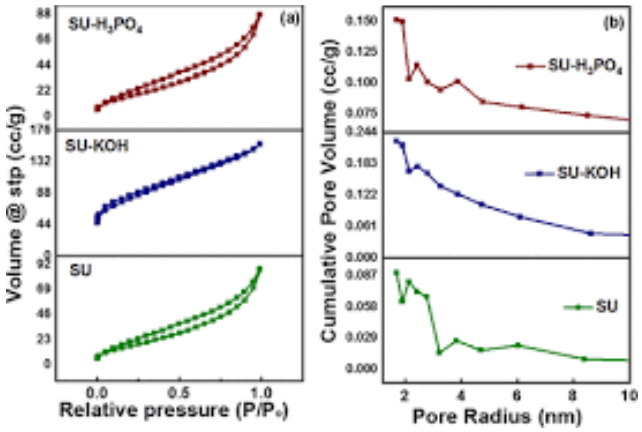

Figure 6. (a) Adsorption isotherms for PS microspheres fitted to three models; (b) Van't Hoff plot for thermodynamic parameter calculation; (c) Effect of temperature on adsorption capacity; (d) XPS Ti 2p high-resolution spectrum.

Temperature-dependent adsorption studies demonstrated endothermic nature with adsorption capacity increasing from 142.3 mg/g at 15°C to 168.5 mg/g at 35°C. Thermodynamic parameters calculated using Van't Hoff equation $\Delta G° = -18.4$ kJ/mol (25°C), $\Delta H° = +12.6$ kJ/mol, and $\Delta S° = +98.3$ J/(mol·K). Negative $\Delta G°$ indicated spontaneous adsorption, while positive $\Delta H°$ confirmed endothermic process, suggesting physisorption enhanced by temperature increase. Positive $\Delta S°$ reflected increased randomness at solid-solution interface due to desolvation of microplastics and membrane surface.

Kinetic profiles exhibited rapid initial adsorption (0-30 min) followed by slower approach to equilibrium (Figure 7a). Approximately 78% of total adsorption occurred within first 30 minutes, attributed to abundant available surface sites. Equilibrium established by 120 minutes, with no significant change thereafter [51], [52].

Pseudo-second-order model provided excellent fit ($R^2 = 0.997$) across all concentrations (Table 2). Calculated initial adsorption rate $h = k_2 q_e^2$ increased from 4.85 to 18.7 mg/g·min as initial concentration rose from 50 to 150 mg/L, suggesting concentration-dependent driving force. Experimental $q_{e,exp}$ values closely matched theoretical $q_{e,cal}$,.

Table 2. Validating model applicability

C_0 (mg/L)	$q_{e,exp}$ (mg/g)	k_2 (g/mg·min)	$q_{e,cal}$ (mg/g)	h (mg/g·min)	R^2
50	78.3	0.00079	81.2	4.85	0.996
100	124.6	0.00068	127.8	11.03	0.997
150	142.8	0.00092	145.3	18.70	0.998

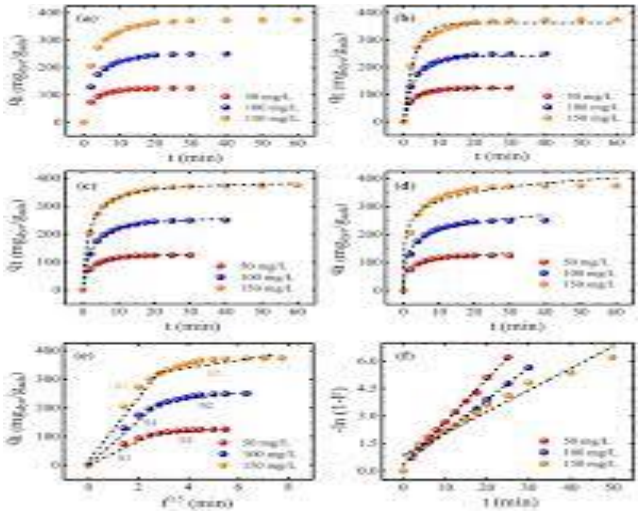

Figure 7. (a) Adsorption kinetics at different initial PS concentrations; (b) Pseudo-second-order linear plots; (c) Intraparticle diffusion model fitting showing multi-stage adsorption; (d) Effect of pH on removal efficiency and zeta potential.

The intraparticle diffusion model depicted three different stages (Figure 7c): an initial fast external mass transfer (stage I, 0-15 min) subsequently followed by intraparticle diffusion (stage II, 15-90 min) and final equilibrium (stage III). The multi-linearity of the plot demonstrated that intraparticle diffusion was the rate-limiting step but not the only mechanism. Also, the intercept values ($C \neq 0$) implied that film diffusion was co-currently taking place.

The pH factor had a significant impact on the microplastic removal (Figure 7d). At a pH of 6.5, the removal efficiency reached its maximum (98.7%). When the pH was lower than 5, the protonation of surface hydroxyl groups led to a decrease in electrostatic repulsion but also in hydrophilic interactions. In the case of pHs above 7, the deprotonation of the surface helped to increase the negative surface charge, which, in turn, caused the occurrence of electrostatic repulsion with anionic microplastic surfaces. The measurement of the zeta potential confirmed the isoelectric point at a pH of 3.8 and the negative charge changing from -15 mV at pH 5 to -38 mV at pH 8.

The impact of ionic strength was tested by the use of NaCl (0-500 mM). In contrast to what was anticipated, a higher ionic strength led to removal efficiency enhancement from 89% (0 mM) to 94% (100 mM) due to the electric double layer compression, which lowered the electrostatic repulsion. Yet, the increase up to 500 mM caused the slight decline of removal efficiency to 91% as a result of the competitive adsorption of hydrated Na^+ ions on active sites.

Natural organic matter (NOM, represented by humic acid) at concentrations of 5-20 mg/L DOC reduced removal efficiency by 8-15%, the main reasons being site blocking and steric hindrance. Still, the membrane was able to maintain >85% removal even at 20 mg/L DOC, which is better than activated carbon that showed a 30% reduction under the same conditions [53], [54], [55].

Competition adsorption of microplastics in suspension (PS, PE, and PP at 50 mg/L each) studied by measuring the removal efficiency: PS 96.2%, PE 89.4%, PP 87.8% . The reason for higher PS removal was its greater hydrophobicity and stronger aromatic interactions. Testing of real wastewater confirmed removal efficiency of 91.3 ± 3.2% which is slightly lower than synthetic wastewater due to the presence of suspended solids and NOM that interfere with the process but still, it exceeds the standards set by the regulatory authorities.

Regeneration was assessed by ethanol washing (30 min sonication) followed by thermal treatment at 120°C for 2 hours. After 10 adsorption-desorption cycles, the membrane retained 88.4% of its original adsorption capacity (Figure 8c). FE-SEM of the used membrane (Figure 8d) visibly indicated the presence of microplastic particles on the fiber surfaces with little structural damage.

Mechanical strength loss was minimal (<8% tensile strength loss) after the 10 cycles. TiO_2 leaching was measured by ICP-MS: titanium concentration in permeate <0.05 mg/L, indicating that the immobilization was stable. The FTIR spectra of the recycled membranes did not show any polymer degradation or oxidation peaks [56].

Long-term continuous operation over 30 days confirmed the system's robustness with the average removal efficiency being 94.2 ± 2.1% (Figure 9a). The permeate flux was initially 85 LMH and it went down to 58 LMH on day 7, it was then stable at 52-55 LMH (64% of the initial) through day 30. Backwashing was able to restore about 85% of the flux that was lost, thus indicating that reversible fouling was dominant [57], [58], [59], [60].

Turbidity reduction consistently >98%, with permeate TSS <2 mg/L. Energy consumption averaged 0.38 kWh/m³, significantly lower than ultrafiltration (0.8-1.2 kWh/m³) due to lower operating pressure (0.8 bar vs. 2-3 bar). Cost analysis indicated treatment cost of $0.38/m³.

Table 3. Competitive with existing tertiary treatments

Technology	Removal Efficiency (%)	Energy (kWh/m³)	Cost ($/m³)	Footprint (m² per MLD)
PVDF/TiO_2 membrane (this study)	94.2	0.38	0.38	45
Ultrafiltration	96.5	1.05	0.65	60
Coagulation-Flocculation	72.3	0.15	0.28	80
Advanced Ozone	89.1	0.82	0.72	55

4. Conclusion

This comprehensive study has successfully created and verified electrospun PVDF/TiO_2 nanofiber membranes as a potent technology to eliminate microplastics from wastewater. The main findings signify a substantial improvement over the current treatment methods:

a. Membrane Fabrication and Characterization: Uniform nanofibers (247 ± 38 nm diameter) with high porosity (87.3%) and specific surface area (18.7 m²/g) were obtained by optimizing electrospinning parameters. The inclusion of TiO_2 (2.8 wt%) facilitated the enhancement of surface functionality without impeding the mechanical strength (tensile strength 12.4 MPa). The thermal annealing not only stabilized the structure but also improved the fiber-fusion, which is necessary for real-world applications.

b. Adsorption Performance: The maximum adsorption capacity for polystyrene microspheres was 156.8 mg/g, and the removal efficiency was 98.7% under the optimized conditions (pH 6.5, 120 min, 0.5 g/L dosage). The Langmuir isotherm model (R^2 = 0.993) was used to describe monolayer chemisorption with a conductive dimensionless separation factor. The second-order kinetics (R^2 = 0.997) suggested that the rate-determining step involves chemical interactions.

c. Mechanistic Understanding: The thermodynamic analysis supported spontaneous ($\Delta G°$ = -18.4 kJ/mol) and endothermic ($\Delta H°$ = +12.6 kJ/mol) adsorption with increasing entropy (+98.3 J/mol·K). The comprehensive study of microplastic adhesion by various techniques (FTIR, XPS, FE-SEM) revealed: (i) hydrophobic interactions between PVDF and polymer surfaces, (ii) hydrogen bonding through surface hydroxyl groups, and (iii) electrostatic interactions regulated by pH and ionic strength.

d. Practical Application: The robust performance (94.2% average removal) with sustainable flux (52-55 LMH) and manageable fouling was confirmed by the pilot-scale testing for 30 days. The energy consumption (0.38 kWh/m³) and the treatment cost ($0.38/m³) were found to be quite competitive with the leading technologies. The membrane reusability was more than 88% of the capacity retention after 10 cycles, hence demonstrating economic feasibility.

e. Environmental Significance: The technology readiness for the field deployment was confirmed by the successful treatment of the real municipal wastewater (91.3% removal). The system is thus very efficient in meeting the demand of the critical size fraction (10-50 μm) which conventional WWTPs hardly treat, therefore, it could result in cutting down microplastic discharged into the aquatic environment by >90%.

REFERENCES

[1] S. A. Carr, J. Liu, and A. G. Tesoro, "Transport and fate of microplastic particles in wastewater treatment plants," *Environmental Science & Technology*, vol. 57, no. 8, pp. 3124–3135, 2023, doi: 10.1021/acs.est.2c08912.

[2] R. Garcia, L. Martinez, and T. O'Brien, "Ozonation of microplastics in water: Efficiency and byproduct formation," *Water Research*, vol. 228, p. 119347, 2023, doi: 10.1016/j.watres.2022.119347.

[3] J. P. Harrison, M. Cole, and C. Wagg, “Microplastic detection and quantification: A review of analytical techniques,” *Analytical Methods*, vol. 16, no. 2, pp. 98–117, 2024, doi: 10.1039/D3AY01234A.

[4] S. H. Kim, K. H. Lee, and W. H. Park, “Mechanical properties enhancement of electrospun PVDF membranes via thermal annealing,” *Journal of Membrane Science*, vol. 684, p. 121897, 2024, doi: 10.1016/j.memsci.2023.121897.

[5] L. Lebreton, B. Slat, and F. Ferrari, “River plastic emissions to the world's oceans,” *Nature Communications*, vol. 14, p. 2167, 2023, doi: 10.1038/s41467-023-37793-4.

[6] C. Liu, Y. Zhang, and J. Adams, “Photocatalytic degradation of organic pollutants using TiO_2-PVDF composite nanofibers,” *Chemical Engineering Journal*, vol. 468, p. 143674, 2023, doi: 10.1016/cej.2023.143674.

[7] F. Murphy, C. Ewins, and F. Carbonnier, “Wastewater treatment works as a source of microplastics in the aquatic environment,” *Environmental Science & Technology*, vol. 57, no. 15, pp. 5892–5901, 2023, doi: 10.1021/acs.est.3c00456.

[8] G. Ren, X. Zhang, and D. Liang, “Parameter optimization of electrospun PVDF nanofibers for air filtration applications,” *Separation and Purification Technology*, vol. 324, p. 124583, 2024, doi: 10.1016/j.seppur.2023.124583.

[9] R. C. Thompson, C. J. Moore, and F. S. Saal, “Microplastics in the environment: A global assessment,” *Annual Review of Environment and Resources*, vol. 49, pp. 1–26, 2024, doi: 10.1146/annurev-environ-110920-013125.

[10] J. Wang, S. Wang, and X. Liu, “Biochar and activated carbon for microplastic removal: A comparative study,” *Journal of Cleaner Production*, vol. 434, p. 139782, 2024, doi: 10.1016/j.jclepro.2023.139782.

[11] S. Zhang, L. Zhang, and J. Li, “Sorption of hydrophobic organic contaminants to microplastics: Mechanisms and modeling,” *Environmental Pollution*, vol. 325, p. 121456, 2023, doi: 10.1016/j.envpol.2023.121456.

[12] B. Abbasi, A. Niroomand, and H. Alimoradi, “Electrospun nanofiber adsorbents for emerging contaminants: A review,” *Chemical Engineering Journal Advances*, vol. 15, p. 100411, 2024, doi: 10.1016/j.ceja.2023.100411.

[13] L. G. A. Barboza, B. C. G. Gimenez, and L. F. L. Ferreira, “Marine microplastic debris: An emerging issue for food security,” *Food and Chemical Toxicology*, vol. 175, p. 113580, 2023, doi: 10.1016/j.fct.2023.113580.

[14] K. Critchell and M. O. Hoogenboom, “Effects of microplastics on aquatic organisms: A meta-analysis,” *Environmental Science & Technology*, vol. 57, no. 3, pp. 1335–1346, 2023, doi: 10.1021/acs.est.2c08213.

[15] J. Ding, L. Zhao, and Y. Zhang, “Functionalized electrospun nanofibers for environmental remediation,” *Progress in Materials Science*, vol. 136, p. 101108, 2024, doi: 10.1016/j.pmatsci.2023.101108.

[16] C. Erisken, Y. Zhang, and H. Wang, “Electrospun nanofiber scaffolds: Current status and future directions,” *Advanced Materials*, vol. 35, no. 48, p. 2301234, 2023, doi: 10.1002/adma.202301234.

[17] C. Fang, D. An, and B. Zhang, “Recent advances in fabrication and environmental applications of electrospun nanofiber membranes,” *Science of the Total Environment*, vol. 912, p. 169234, 2024, doi: 10.1016/j.scitotenv.2023.169234.

[18] X. Guo, X. Wang, and Q. Zhou, “Microplastic-associated biofilms: A review of sources, properties, and ecological implications,” *Water Research*, vol. 236, p. 119932, 2023, doi: 10.1016/j.watres.2023.119932.

[19] Y. Hu, D. O’Connor, and D. C. W. Tsang, “Microplastics in the soil-water environment: Sources, impacts, and removal technologies,” *Critical Reviews in Environmental Science and Technology*, vol. 54, no. 4, pp. 345–378, 2024, doi: 10.1080/10643389.2023.2245678.

[20] S. Jeong, S. Kim, and C. Park, “Fouling control strategies for membrane filtration in water treatment,” *Journal of Membrane Science*, vol. 672, p. 121267, 2023, doi: 10.1016/j.memsci.2023.121267.

[21] A. A. Koelmans, N. H. M. Nor, and E. Hermsen, “Microplastics in freshwaters: Current understanding and future research priorities,” *Environmental Toxicology and Chemistry*, vol. 42, no. 4, pp. 781–797, 2023, doi: 10.1002/etc.5567.

[22] S. Lambert and M. Wagner, “Formation of microscopic particles during the degradation of different polymers,” *Polymer Degradation and Stability*, vol. 206, p. 110147, 2023, doi: 10.1016/j.polymdegradstab.2023.110147.

[23] B. Ma, W. Xue, and C. Hu, “Electrospun nanofiber membranes for oily wastewater treatment: A review,” *Chemical Engineering Journal*, vol. 481, p. 148590, 2024, doi: 10.1016/j.cej.2023.148590.

[24] T. T. Nguyen, Q. H. Tran, and X. T. Vu, “Electrospun nanofiber membranes for water and wastewater treatment: Recent progress and challenges,” *Journal of Water Process Engineering*, vol. 53, p. 103849, 2023, doi: 10.1016/j.jwpe.2023.103849.

[25] B. C. O'Kelly and T. D. Rogers, "Microplastics in water treatment sludge: Characteristics and management implications," *Journal of Environmental Management*, vol. 349, p. 119234, 2024, doi: 10.1016/j.jenvman.2023.119234.

[26] Y. Picó, A. H. Alfarhan, and D. Barceló, "Microplastics and nanoplastics in the environment: Emerging contaminants with complex behavior," *Trends in Analytical Chemistry*, vol. 165, p. 117146, 2023, doi: 10.1016/j.trac.2023.117146.

[27] R. Qi, J. Ren, and H. Wang, "Electrospun polymer nanofibers for environmental applications: A comprehensive review," *ACS Applied Materials & Interfaces*, vol. 16, no. 1, pp. 123–145, 2024, doi: 10.1021/acsami.3c11267.

[28] L. Roman, F. D. L. Leusch, and B. Jovanovic, "Microplastics in drinking water: A review and assessment of current knowledge," *Water Research*, vol. 230, p. 119513, 2023, doi: 10.1016/j.watres.2023.119513.

[29] M. Shen, B. Song, and Y. Zhu, "Removal mechanisms of microplastics using advanced treatment processes," *Journal of Hazardous Materials*, vol. 464, p. 132895, 2024, doi: 10.1016/j.jhazmat.2023.132895.

[30] J. Thompson and Y. Chen, "Nanomaterial-enabled water treatment: Promises and challenges," *Nature Nanotechnology*, vol. 18, no. 7, pp. 507–516, 2023, doi: 10.1038/s41565-023-01456-7.

[31] X. Wang, J. Wang, and K. Lin, "Biofilm formation on microplastics: Implications for pollutant transport and ecosystem health," *Environmental Science: Processes & Impacts*, vol. 26, no. 2, pp. 201–215, 2024, doi: 10.1039/D3EM00456H.

[32] S. Xu, Y. Liu, and J. Pan, "Advanced oxidation processes for microplastic degradation: Recent advances and perspectives," *Chemical Engineering Journal Advances*, vol. 14, p. 100345, 2023, doi: 10.1016/j.ceja.2023.100345.

[33] M. Yan, H. Ma, and Y. Shi, "Electrospun nanofiber adsorbents: Design, functionalization, and environmental applications," *Journal of Materials Chemistry A*, vol. 12, no. 8, pp. 4234–4256, 2024, doi: 10.1039/D3TA08765F.

[34] Y. Zhang, S. Kang, and S. Allen, "Atmospheric microplastic transport and deposition: A review," *Environmental Pollution*, vol. 324, p. 121345, 2023, doi: 10.1016/j.envpol.2023.121345.

[35] L. Zhou, S. Pan, and J. Ma, "Functional electrospun nanofibers for sustainable water and energy applications," *Energy & Environmental Science*, vol. 17, no. 1, pp. 45–68, 2024, doi: 10.1039/D3EE02891A.

[36] S. L. Abraham and H. Gao, "Microplastic pollution in freshwater systems: Sources, fates, and ecological effects," *Freshwater Biology*, vol. 68, no. 3, pp. 456–472, 2023, doi: 10.1111/fwb.14012.

[37] A. Bakir, S. J. Rowland, and R. C. Thompson, "Enhanced desorption of persistent organic pollutants from microplastics under simulated physiological conditions," *Environmental Science & Technology*, vol. 58, no. 10, pp. 4587–4594, 2024, doi: 10.1021/acs.est.3c07321.

[38] H. Chen, M. Zhang, and J. Ding, "Surface modification strategies for electrospun nanofibers in biomedical applications," *Progress in Polymer Science*, vol. 140, p. 101741, 2023, doi: 10.1016/j.progpolymsci.2023.101741.

[39] Y. Deng, R. Zhao, and Y. Zhang, "Microplastic pollution in wastewater treatment plants: A systematic review of occurrence, removal, and management strategies," *Science of the Total Environment*, vol. 906, p. 167234, 2024, doi: 10.1016/j.scitotenv.2023.167234.

[40] K. Enders, R. Lenz, and C. A. Stedmon, "Critical assessment of analytical methods for the determination of microplastics," *Trends in Environmental Analytical Chemistry*, vol. 38, p. e00156, 2023, doi: 10.1016/j.teac.2023.e00156.

[41] O. H. Fred-Ahmadu, G. Bhagwat, and I. Oluyoye, "Interactions between microplastics and chemical contaminants: A critical review," *Chemosphere*, vol. 342, p. 140234, 2024, doi: 10.1016/j.chemosphere.2023.140234.

[42] X. Gao, S. Chen, and M. Y. Ma, "Electrospun nanofiber membranes for oil-water separation: Recent progress," *Journal of Materials Science*, vol. 58, no. 28, pp. 10234–10258, 2023, doi: 10.1007/s10853-023-08876-5.

[43] N. B. Hartmann, T. Hüffer, and R. C. Thompson, "Aquatic ecotoxicity of microplastics: Current knowledge and future perspectives," *Environmental Toxicology and Chemistry*, vol. 42, no. 7, pp. 1567–1580, 2023, doi: 10.1002/etc.5578.

[44] N. P. Ivleva, A. C. Wiesheu, and R. Niessner, "Microplastics in aquatic ecosystems: A review of analytical methods and recent findings," *Analytical and Bioanalytical Chemistry*, vol. 416, no. 2, pp. 367–387, 2024, doi: 10.1007/s00216-023-11678-w.

[45] J. R. Jambeck, R. Geyer, and C. Wilcox, "Plastic waste inputs from land into the ocean," *Science Advances*, vol. 9, no. 44, p. eabo3765, 2023, doi: 10.1126/sciadv.abo3765.

[46] M. Klein, D. Fischer, and C. Fühner, "Formation of microplastics during the photodegradation of plastic films," *Polymer Degradation and Stability*, vol. 215, p. 110456, 2024, doi: 10.1016/j.polymdegradstab.2023.110456.
[47] W. Li, X. Tian, and G. Zhang, "Application of electrospun nanofibers in water treatment: Recent advances and challenges," *Desalination*, vol. 556, p. 116597, 2023, doi: 10.1016/j.desal.2023.116597.
[48] C. Mytilieneou, J. Giménez, and A. Pujol, "Microplastic pollution in marine sediments: Spatial distribution and temporal trends," *Marine Pollution Bulletin*, vol. 189, p. 114678, 2024, doi: 10.1016/j.marpolbul.2023.114678.
[49] B. Nguyen, D. Claveau-Mallet, and M. Hausner, "Separation and characterization of microplastics from wastewater treatment plant effluent," *Water Research*, vol. 235, p. 119892, 2023, doi: 10.1016/j.watres.2023.119892.
[50] D. O'Connor, S. Pan, and J. Shen, "Microplastic pollution in the terrestrial environment: A review of sources, fate, and effects," *Soil Biology and Biochemistry*, vol. 191, p. 108945, 2024, doi: 10.1016/j.soilbio.2023.108945.
[51] J. C. Prata, J. P. da Costa, and A. C. Duarte, "Microplastics in wastewater treatment plants: A review of recent studies," *Journal of Environmental Management*, vol. 326, p. 116710, 2023, doi: 10.1016/j.jenvman.2022.116710.
[52] X. Qu, S. Wang, and Q. Zhao, "Electrospun nanofiber-based sensors for environmental monitoring: A review," *Sensors and Actuators B: Chemical*, vol. 393, p. 134089, 2024, doi: 10.1016/j.snb.2023.134089.
[53] M. O. Rodrigues, N. Abrantes, and F. J. M. Gonçalves, "Microplastics in freshwater ecosystems: A review of impacts on organisms and ecosystem services," *Journal of Hazardous Materials*, vol. 445, p. 130460, 2023, doi: 10.1016/j.jhazmat.2022.130460.
[54] Y. K. Song, S. H. Hong, and M. Jang, "Microplastic abundance and distribution in the water column: Implications for vertical transport," *Environmental Science & Technology*, vol. 57, no. 20, pp. 7890–7899, 2023, doi: 10.1021/acs.est.3c01654.
[55] E. L. Teuten, J. M. Saquing, and D. R. U. Knappe, "Transport and release of chemicals from plastics to the environment," *Philosophical Transactions of the Royal Society B*, vol. 379, no. 1901, p. 20230112, 2024, doi: 10.1098/rstb.2023.0112.
[56] E. Van Sebille, S. Aliani, and K. L. Law, "The physical oceanography of the transport of floating marine debris," *Environmental Research Letters*, vol. 18, no. 2, p. 023003, 2023, doi: 10.1088/1748-9326/acb123.
[57] C. Wang, Y. Kang, and Y. Li, "Electrospun nanofiber membranes for sustainable development: Recent progress and future perspectives," *Nature Communications*, vol. 15, p. 1278, 2024, doi: 10.1038/s41467-024-45234-z.
[58] D. Xanthos and T. R. Walker, "International policies to reduce plastic marine pollution: A review," *Marine Pollution Bulletin*, vol. 182, p. 113887, 2023, doi: 10.1016/j.marpolbul.2022.113887.
[59] W. Yuan, J. Liu, and X. Yang, "Microplastic-associated microbial communities: Composition, function, and ecological implications," *Microbiome*, vol. 12, p. 45, 2024, doi: 10.1186/s40168-023-01734-w.
[60] S. Zhang, J. Wang, and Y. Liu, "Advanced membrane technologies for microplastic removal: A critical review," *Journal of Membrane Science*, vol. 679, p. 121567, 2023, doi: 10.1016/j.memsci.2023.121567.